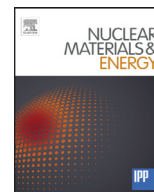




Contents lists available at ScienceDirect

Nuclear Materials and Energy

journal homepage: www.elsevier.com/locate/nme

Behavior of tungsten fiber-reinforced tungsten based on single fiber push-out study

B. Jasper^{a,*}, S. Schoenen^b, J. Du^a, T. Hoeschen^c, F. Koch^c, Ch. Linsmeier^a, R. Neu^{c,d}, J. Riesch^c, A. Terra^a, J.W. Coenen^a

^a Forschungszentrum Jülich GmbH, Institut für Energie- und Klimaforschung, Jülich, Germany

^b Forschungszentrum Jülich GmbH, Zentralinstitut für Engineering, Elektronik und Analytik - Engineering und Technologie, Jülich, Germany

^c Max-Planck-Institut für Plasmaphysik, Garching, Germany

^d Technische Universität München, Boltzmannstrasse 15, Garching 85748, Germany

ARTICLE INFO

Article history:

Received 16 November 2015

Revised 7 March 2016

Accepted 21 April 2016

Available online xxx

PACS:

28.52.Fa

28.52.Lf

81.05.Ni

81.20.Ev

Keywords:

ICFRM: tungsten

Composite

Fiber

Push-out

ABSTRACT

To overcome the intrinsic brittleness of tungsten (W), a tungsten fiber-reinforced tungsten-composite material (W_f/W) is under development. The composite addresses the brittleness of W by extrinsic toughening through the introduction of energy dissipation mechanisms. These mechanisms allow the reduction of stress peaks and thus improve the materials resistance against crack growth. They do not rely on the intrinsic material properties such as ductility. By utilizing powder metallurgy (PM) one could benefit from available industrialized approaches for composite production and alloying routes. In this contribution the PM method of hot isostatic pressing (HIP) is used to produce W_f/W samples containing W fibers coated with an Er_2O_3 interface. Analysis of the matrix material demonstrates a dense tungsten bulk, a deformed fiber and a deformed, but still intact interface layer. Metallographic analysis reveals indentations of powder particles in the interface, forming a complex 3D structure. Special emphasis is placed on push-out tests of single fiber HIP samples, where a load is applied via a small indenter on the fiber, to test the debonding and frictional properties of the Er_2O_3 interface region enabling the energy dissipation mechanisms. Together with the obtained experimental results, an axisymmetric finite element model is discussed and compared to existing work. In the HIP W_f/W composites the matrix adhesion is rather large and can dominate the push-out behavior. This is in contrast to the previously tested CVD produced samples.

© 2016 The Authors. Published by Elsevier Ltd.

This is an open access article under the CC BY-NC-ND license (<http://creativecommons.org/licenses/by-nc-nd/4.0/>).

1. Introduction

When considering a future fusion power plant multiple intertwined issues need to be evaluated. Some of the main challenges are linked to the materials exposed to the plasma and their lifetime considerations. An important challenge are effects caused by thermal fatigue by transient heat loading, as typically 10^9 (30 Hz) thermal transients (ELMs) during one full power year of operation are to be expected. Erosion of the first wall and the divertor will in addition require a significant armor thickness or short exchange intervals, while high-power transients need strong mitigation efficiency to prevent damage of the plasmafacing components [1]. Therefore materials with advanced properties in areas ranging

from mechanical strength to thermal properties are required [2]. Tungsten (W) is currently the main candidate material for the first wall of a fusion reactor as it is resilient against erosion, has the highest melting point of any metal and shows rather benign behavior under neutron irradiation [3], as well as low tritium retention. But extrinsic toughening mechanisms are required, since the high thermal and neutron loads during operation lead to an embrittlement of the tungsten materials. Composite approaches allow the combination of beneficial properties and would therefore be ideal to enhance material parameters and mitigate damage effects. Already today smart materials, fiber composites and alloys which adapt to the operational scenario are possible [2].

1.1. Tungsten fiber-reinforced tungsten W_f/W

One major disadvantage of W is its brittleness below the ductile-to-brittle transition temperature (DBTT), which ranges from

* Corresponding author.

E-mail address: b.jasper@fz-juelich.de (B. Jasper).

<http://dx.doi.org/10.1016/j.nme.2016.04.010>

2352-1791/© 2016 The Authors. Published by Elsevier Ltd. This is an open access article under the CC BY-NC-ND license (<http://creativecommons.org/licenses/by-nc-nd/4.0/>).

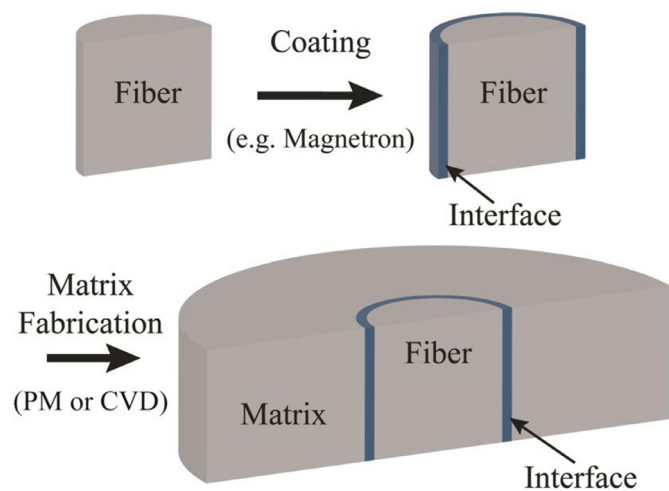


Fig. 1. Basic structure of a single-fiber W_f/W containing the interface, a fiber and the matrix.

400–700 K [4], depending on the preparation history of the material. To circumvent the issue of brittleness if using W, different composite approaches are investigated. Tungsten fiber-reinforced tungsten (W_f/W), as one example, utilizes fiber-reinforcement and comprises of a pure W matrix and an interface layer around a W fiber [5,6]. The basic idea is to introduce extrinsic toughening mechanisms which allow for crack energy dissipation. This is the only way to enhance the toughness in intrinsic brittle materials and commonly used to toughen ceramics [7]. A basic strategy to achieve pseudo-ductility is the incorporation of fibers and a weak interface into a matrix, which needs extensive development and validation [8]. In case of W, a W fiber-reinforced W composite material (W_f/W) can be used to overcome brittleness issues (Fig. 1). The incorporated fibers enable extrinsic mechanisms, thus stress peaks at crack tips can be reduced and further crack growth prevented.

Other options include composite laminates made of commercially available raw materials [9,10]. The link between W_f/W and laminates is the similarity of fibers and foils. Both show a special microstructure of highly deformed and elongated grains, hence showing high strength and ductility even at room temperature [11,12,13]. Accordingly, even in the brittle regime, below the DBTT, these materials allow for a certain tolerance towards cracking and damage in general. Even if a crack has been initiated inside the composite material the extrinsic energy dissipation mechanisms allow further load to be applied towards the component. In comparison, conventional tungsten would fail immediately. After reaching the ultimate strength the mechanisms also lead to a controlled failure rather than a catastrophic one in the brittle case. Assuming embrittlement by high-temperature operation and neutrons however it can be expected that ductility will be lost.

W_f/W in contrast to W-laminates hence has the benefit of utilizing extrinsic mechanisms and still working in the embrittled case [14]. First W_f/W samples have been produced, showing extrinsic toughening mechanisms similar to those of ceramic materials [15,16]. They exhibit the necessary mechanisms to mitigate effects of operational embrittlement due to neutrons and high operational temperatures.

A component based on W_f/W can be produced with both chemical vapor deposition (CVD) [6] and a powder metallurgical path through hot isostatic pressing [17] (Fig. 3). Crucial in both cases is the interface between fiber and matrix, since both are made out of tungsten. The interface is typically a thin layer (Fig. 1) with targeted properties: weak enough to enable the toughening mecha-

nism, as strong as possible to maximize the dissipated energy [5]. This is an idea based on enabling pseudo-ductile fracture in inherently brittle material, e.g. SiC ceramics [18].

2. Single fiber W_f/W characterisation

The main experimental characterization method of this work is the push-out test. It provides a quantitative insight into important parameters of the fiber-interface-matrix system, e.g. the interfacial shear strength (τ_d). The load-displacement curve, obtained during the test, displays several important features, e.g. the load that is needed to initially break or debond the interface or the maximum load which the sample is able to withstand before complete debonding. For W_f/W samples produced via chemical vapor infiltration this test was extensively used [19] and important parameters characterizing the interface were retrieved. Depending on the underlying theory one can for example determine τ_d by obtaining the maximum load for a series of samples from the same batch with different thicknesses (H) by fitting according to Eq. 1. A more basic approach can be found in [20].

$$F_{max} = \pi \cdot \frac{d_f * \tau_d}{\alpha_2} \cdot \tanh(\alpha_2 \cdot H) \quad (1)$$

where F_{max} is the maximum load, d_f the diameter of the fiber, α_2 the elastic constant, a parameter in shear-lag theory and τ_d the interfacial shear strength.

2.1. Sample preparation and experimental

The samples presented in this work are hot isostatically pressed (HIPed) in an argon atmosphere at 200 MPa for 4 h, if not indicated otherwise. Carbon heating filaments are used to achieve the desired temperatures of 1500 °C. Powder provided by Plansee SE was chosen to produce the PM W_f/W samples. The mean particle diameter of the powders is $10.60 \pm 7.78 \mu\text{m}$. The fibers used for this work are made of undoped and pure tungsten with a diameter of 150 μm (made available by Osram GmbH) and possess a as produced tensile strength of typically 2900 MPa. The fibers are not stabilized against recrystallization by potassium doping, hence tend to lose their ductility at temperatures above 1000 °C. For more details on the sample production refer to [17] and for detail on the actual fiber to [13,16].

Before testing and analysis, all samples were prepared in size and shape appropriate for the specific method. In addition, all samples are polished with a Saphier 550 - Rubin 520 polishing machine (ATM GmbH) using silicon carbide paper and 3 μm and 1 μm diamond polishing suspensions for the final polishing steps. A $K_3[\text{Fe}(\text{CN})_6]$ etching solution is used to reveal the grain structure and enhance the visibility of the fiber for precise positioning before the push-out test. All scanning electron microscopy (SEM) images presented here are either taken with a DSM 982 Gemini or a Crossbeam 540 Gemini II (Carl Zeiss AG), which is also a focused ion beam (FIB) device. Density measurements are carried out on a pure W section of the sample after Archimedes principle with a Cubis MSA225S scale and the density measurement kit YDK01 (Satorius AG) in 99.9% ethanol. All W_f/W single fiber samples are showing a density of 99% or more.

2.2. Push-out test

The push-out tests are carried out with the help of a setup containing a special sample holder (Fig. 2(a)) and a micro-indenter attached to an Instron 3342 universal testing machine (Instron GmbH) with a 500 N load cell. The fiber of the single fiber push-out samples, polished on both sides, is positioned over a small hole (diameter $L = 0.2 \text{ mm}$) in the sample holder and then carefully

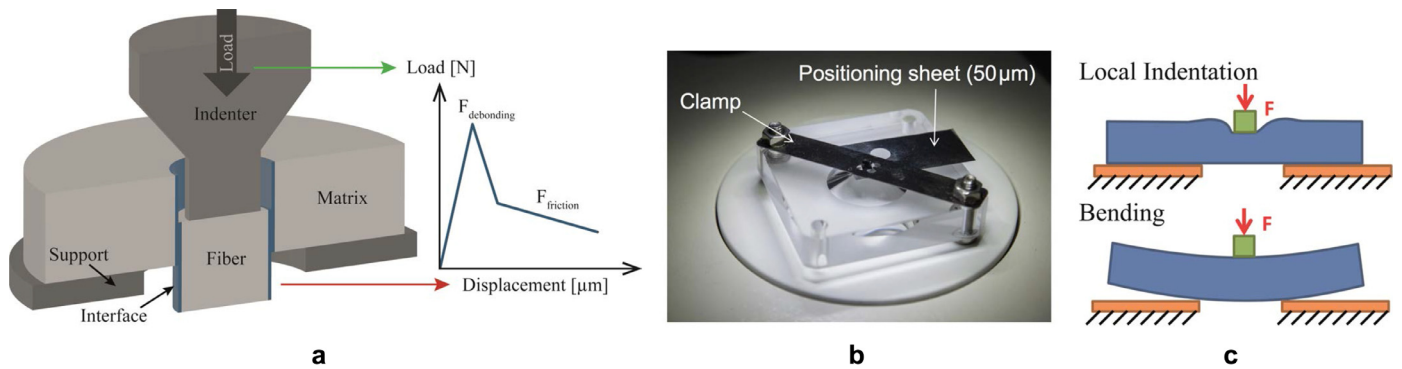


Fig. 2. (a) Push-out procedure including the sample geometry, setup and push-out curve, (b) the glass sample holder and (c) the potential issues.

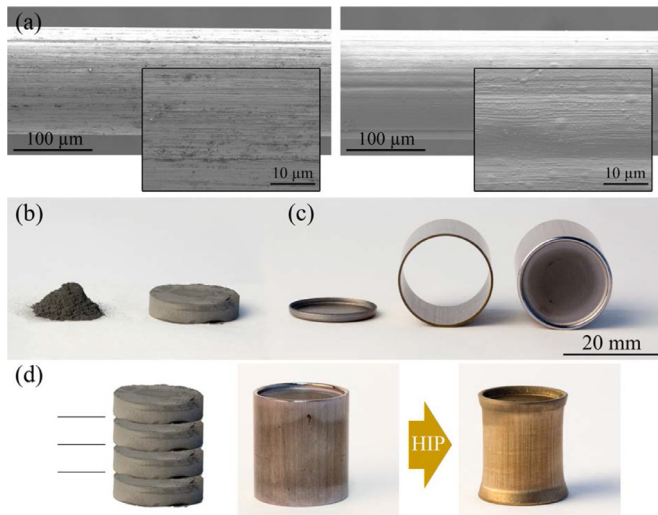


Fig. 3. The manufacturing process of HIPed W_f/W : (a) Uncoated (left) and coated fiber (right), (b) W powder and the prepressed greenbody tablets, (c) tantalum lid and cylinder and assembled tantalum HIP capsule, (d) schematic of fibers and tablets a HIP capsule is containing and a HIPed capsule.

placed under the indenter (diameter $120\ \mu\text{m}$). By then applying a load on the fiber a force–displacement curve can be obtained (Fig. 2(a)). These curves are then corrected by $0.66\ \mu\text{m}/\text{N}$ to compensate for the effect of the imperfect stiffness of the machine and the test setup. The total displacement during the test was kept to roughly $H/2$.

2.2.1. Issues

As will be discussed in the following section sections the setup and the size of the sample can be crucial when trying to extract the interface parameters. Especially the ratio between sample thickness (H) and the support (L), in our case the diameter of the hole of the sample holder, can be crucial for obtaining relevant data [21]. Fig. 2(c) displays the basic issues that can arise. On one side if the sample is thin, its thickness in the order of the support width, bending of the sample can occur and drastically change the stress state of the specimen and therefore influence interfacial parameters. On the other side if the sample is too thick, depending on the interface, the frictional force and adhesion might be too strong enough to enable cracking of the matrix before debonding can take place.

2.2.2. Experimental results

To experimentally evaluate the impact of the thickness (H) of the single fiber HIP W_f/W samples on the behavior during the push-out test, samples with a thickness varying from $600\ \mu\text{m}$ to

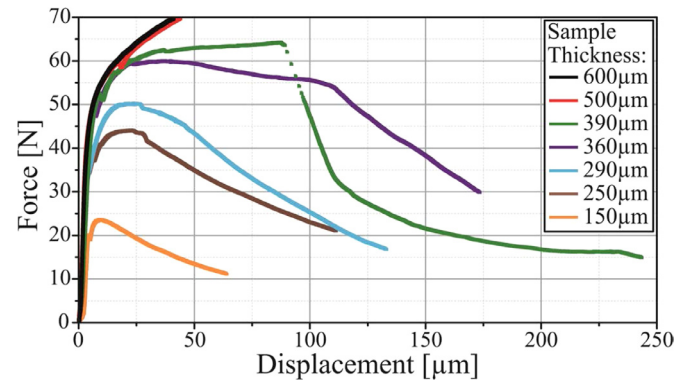


Fig. 4. Force–displacement curves for single fiber samples with different thicknesses. Thick samples exhibit drastic plastic deformation and could not be pushed out. The matrix of the samples with $390\ \mu\text{m}$ thickness failed after a displacement of $90\ \mu\text{m}$ (Fig. 5). For thinner samples a complete push-out curve can be recorded.

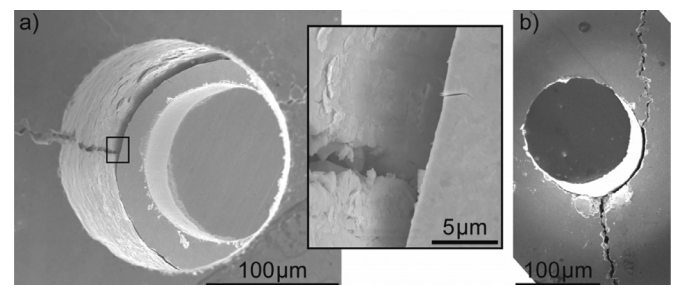


Fig. 5. SEM images of pushed-out sample with $390\ \mu\text{m}$ thickness. (a) Visible are the imprint of the indenter in the fiber and the crack running through the matrix but leaving the fiber intact. The insert shows minor cracks in the fiber and the interface attached to the matrix. (b) The back of the sample also shows the large crack running through the matrix of the sample.

$150\ \mu\text{m}$ were prepared. In Fig. 4 representative force–displacement curves show that the maximum force clearly depends on the thickness of the sample. It was not possible to reach complete debonding ($500\ \mu\text{m}$) or even initial debonding ($600\ \mu\text{m}$) for thicker samples without risking the destruction of the indenter, going beyond $70\ \text{N}$. After settling effects at forces up to $5\ \text{N}$, all samples display a linear elastic regime up to roughly $30\ \text{N}$. A non-linear behavior is noticeable above this threshold. For samples below $400\ \mu\text{m}$ of thickness complete debonding was reached and a full push-out curve recorded.

As can be seen in Fig. 4, the shape of the curve for the $390\ \mu\text{m}$ sample is completely different than those of the thinner samples. This can be explained by further investigation of the morphology of the samples after the push-out test. In Fig. 5 a crack through the

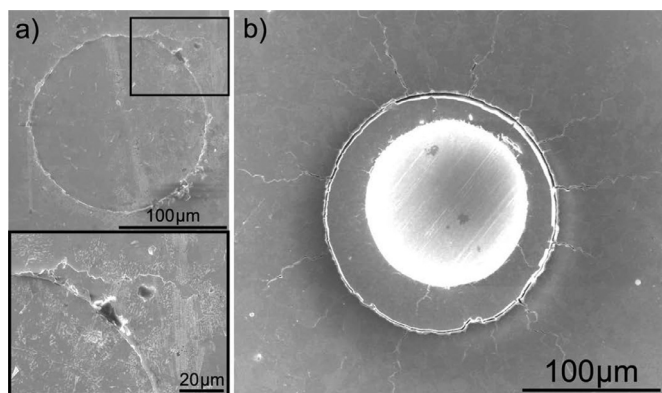


Fig. 6. SEM images of a 500 μm sample. (a) Back: Some cracks originating at the interface are visible but no push-out can be observed. (b) Heavily deformed front of the sample with deep imprint of the indenter. A crack network is formed in both fiber and matrix.

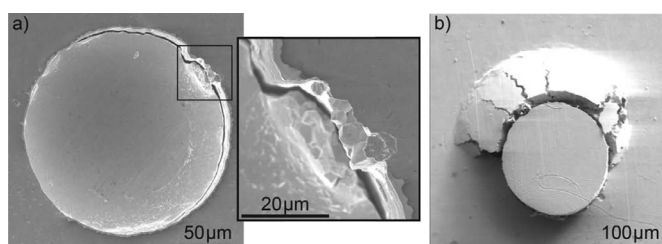


Fig. 7. (a) Front of a thin sample ($H = 150 \mu\text{m}$) with no indentations, but cracking between matrix and fiber due to missing interface. (b) Sample HIPed at $1600 \text{ }^\circ\text{C}$ ($H = 220 \mu\text{m}$) pushed with a sample holder with a larger support hole ($L = 0.4 \text{ mm}$) resulting in cracking of the matrix on the side facing the sample holder.

matrix of the whole sample is visible. The cracking itself caused the large load drop after $90 \mu\text{m}$ displacement. In addition, an imprint of the indenter in the fiber is visible. Furthermore, the insert shows that due to the plastic deformation cracking occurred at the edge of the fiber.

The surface morphology of thick samples ($H = 500 \mu\text{m}$ and $600 \mu\text{m}$), where push-out was not reached, display an even deeper imprint and heavier deformation (Fig. 6). The load was large enough to cause cracking of both fiber and matrix. Thinner samples in contrast did not show signs of cracking on the front/indenter side. For thin samples that were tested with a sample holder with a larger hole ($L = 0.4 \text{ mm}$), resulting in less support, cracking of the matrix at the back side, facing the sample holder, can be observed (Fig. 7(b)). During SEM investigation also effects of an imperfect interface are visible. As shown in Fig. 7(a) and in the corresponding insert, brittle fracture between matrix and fiber can be found. Furthermore, all samples exhibited debonding mainly at the fiber-interface boundary, leaving most of the interface material attached to the matrix and intact after the push-out test. Nevertheless, on pushed-out fibers flakes of the interface material was found.

When measuring the diameter of the fiber, it was seen that it increased by as much as 10% when compared to the as prepared state before HIP indicating deformation as consequence of the high pressures.

3. Modeling of single fiber push-out

The common way to interpret the experimental results of the push out tests, as done for example by Shetty or Liang and Hutchinson [22,23], is to apply analytical models and to determine the associated parameters by a fitting procedure (Eq. 1). To create a deeper understanding of the mechanisms that are acting during

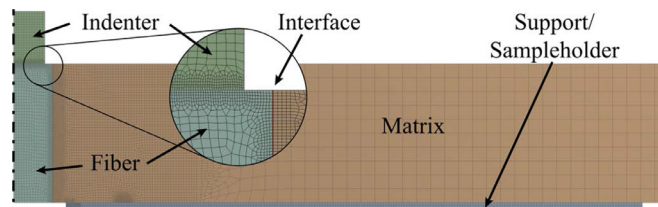


Fig. 8. Axisymmetric 2D FE-model of the push-out test and its structure.

the different phases of a push-out test modeling activities that accompany the experimental work have been initiated. The applied finite element method (FEM) is a well established method to treat a wide range of mechanical problems of scientific and industrial applications and also to deepen the understanding of push-out tests [24].

3.1. Model setup

ANSYS V15.0 was used for the finite element calculations. The model (Fig. 8) consists of 2D elements with quadratic displacement behavior (PLANE183) and axisymmetric formulation. For the brittle matrix a linear-elastic material model is assumed. The material model of the fiber considers plasticity. The flow curve of this material model was approximated based on tensile tests of fibers and tomographic in-situ measurements of the fiber deformation in a single-fiber composite [14]. It has to be noted that these single-fiber W_f/W samples were produced via Chemical Vapor Deposition in contrast to the presented hot isostatic pressed samples presented in the experimental section above. The debonding behavior of the interface is represented by a cohesive contact which contains parameters for the strength properties and interfacial fracture energies. Parameters for an interface of erbium oxide (Er_2O_3) with a thickness of 600 nm [5] were taken as starting point to parametrize the cohesive contact between fiber and matrix. Some parameters of the contact had to be adjusted to obtain a reasonable physical behavior of the simulation.

3.2. Stress states of the interface

Push-out tests performed with composites with dissimilar materials of fiber and matrix sustain a significant load even after complete debonding. This force is most commonly explained with a pressure of the interface caused by residual stresses. These residual stresses are typically induced by different coefficients of thermal expansion or shrinking of the matrix as a result of a chemical reaction (curing of resin).

In the case of W_f/W no thermal mismatch between fiber and matrix exists, since both are pure tungsten and the influence of the thin interface can be neglected [19]. This is a clear difference when discussing W_f/W in comparison to SiC or other composites with dissimilar materials for fiber and matrix. Du proposed that normal interface pressure could also be induced by surface roughness during the push-out test (asperity caused interface pressure). Nevertheless, push-out tests of CVD and HIP W_f/W show a behavior after completion of debonding that is quite similar to push-out tests where an initial interface pressure is known to be present. This leads to the assumption that a certain amount of interface pressure also exists in W_f/W . The cause for this initial interface pressure is not yet clarified. In order to take this observation into account an initial interface pressure is considered in the model.

When pushing the indenter against the top of the fiber additional stress components (normal pressure and shear stresses) arise in the interface. They can be separated by their cause (Fig. 9). The final stress profile is the sum of the different components and

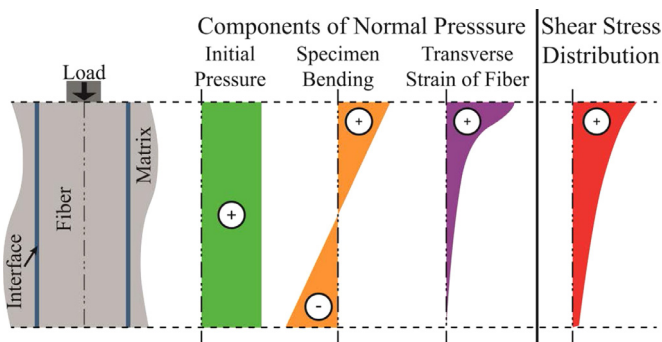


Fig. 9. Schematic of the components of the normal pressure and the shear stress distribution of the fully bonded interface.

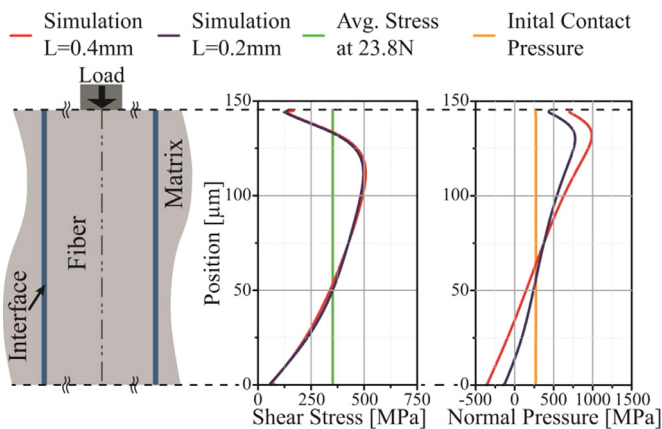


Fig. 10. Simulated interface stresses of an ideal bonded interface for a thin specimen with $145\ \mu\text{m}$ thickness and an indenter load of $23.8\ \text{N}$ for a support thickness L of $0.4\ \text{mm}$ and $0.2\ \text{mm}$. Sketch not to scale.

depends on the elastic and geometrical properties of the specimen and the load applied by the indenter.

During the push-out test the specimen is placed on a holder containing a hole with typical diameters of $0.2\text{--}0.4\ \text{mm}$ for a fiber diameter of $150\ \mu\text{m}$. For details on the push-out test please refer to Section 2.2. The difference of the diameters of indenter and the hole in the specimen holder leads to a bending of the specimen and the corresponding normal pressure with compression at the top and tension at the bottom of the specimen. This component increases for thinner specimens and larger hole diameters. The transverse strain of the fiber due to the poisson effect leads to an additional component of the interface pressure. Its maximum value is near the top of the specimen and it decreases with increasing distance to the top.

In contrast, the shear stress distribution along the fiber length for the fully bonded case depends on the elastic properties of the fiber, interface and matrix and cannot be split into different components, since it is caused by applied load of the indenter. The variation of the shear stress along the fiber length is shown schematically in Fig. 9. Fig. 10 shows the computed shear stress and normal pressure distribution for a sample with $145\ \mu\text{m}$ thickness and an applied load of $23.8\ \text{N}$ for two different hole diameters ($L = 0.2\ \text{mm}$ and $0.4\ \text{mm}$) of the specimen holder. It can be seen that the hole diameter has an influence on the occurrence and the magnitude of the normal pressure at the top and the bottom of the specimen. In contrast, the influence on the shear stress can be neglected.

To minimize the influence of bending also the behavior of thicker samples was simulated. Fig. 12(a) compares force-displacement curves of push-out experiments of CVD W_f/W

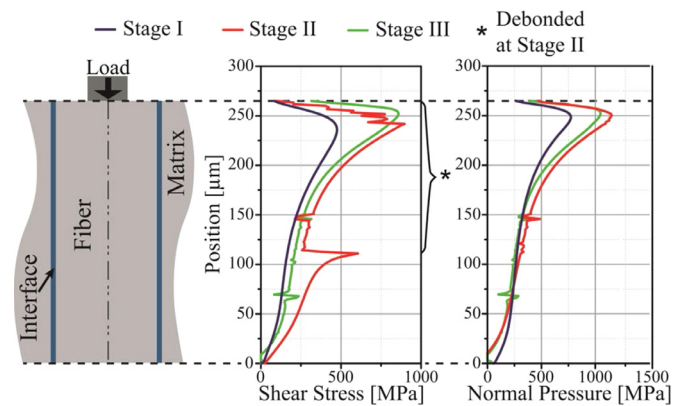


Fig. 11. Simulated interface stresses for a sample with $H = 265\ \mu\text{m}$ and $L = 0.2\ \text{mm}$ during the three phases of a push-out test. Sketch not to scale.

[5] with simulations of a debonding interface. A closer look at the first $2\ \mu\text{m}$ of indenter displacement (Fig. 12(b)) reveal the three phases of a push-out test, also visible in the simulated force-displacement curve. After linear elastic deformation of the specimen the initiation of debonding leads to a non-linear decrease of the slope at $0.85\ \mu\text{m}$. Less than $0.5\ \mu\text{m}$ of further indenter displacement are necessary to reach complete debonding at $1.3\ \mu\text{m}$. During the debonding process the stress state in the interface changes.

Fig. 11 shows the distribution of the shear stress and normal pressure of the interface at the three stages described above. The corresponding indenter displacements of $0.5\ \mu\text{m}$, $1\ \mu\text{m}$ and $1.5\ \mu\text{m}$ are labeled in Fig. 12(b). During the debonding process, the interface can be split into a debonded area with frictional behavior and a still bonded area. The debonding starts near the top of the specimen and extends towards the bottom until the debonding process is completed. The length of the debonded zone at stage II can be easily identified with the help of the shear stress distribution (Fig. 11). At the boundary between frictional and bonded interface a singularity (crack tip) leads to a shear stress peak. Both, the bonded and frictional part of the interface carry a significant portion of the load introduced by the indenter. At stage II 72% of the load is transmitted by friction. Without this contribution a further load increase after the initiation of debonding would not be possible.

4. Discussion, conclusion and outlook

As can be seen in Fig. 4 there is a clear specimen-thickness dependence of the push-out test. The high force needed for thick samples leads to indentation of the indenter. For thin samples bending influences the stress state and therefore the results of the push-out test. What is more surprising is the multitude of effects further influencing the resulting push-out curve. As shown in the modeling section (Section 3) the frictional properties of the interface are not only significantly influencing the purely frictional phase of the push-out test but the debonding phase as well. Where a large fraction of the load is transmitted via friction. The effects related to friction are responsible for the ability of the single fiber specimen to withstand increasing loads during the second stage of the push-out test. When considering the frictional part alone, the initial normal pressure and therefore residual stresses in the material are also playing an important role. The origin and magnitude of the residual stress in this system is not known, since a mismatch of the thermal expansion coefficient between the tungsten fiber and the tungsten matrix is not given.

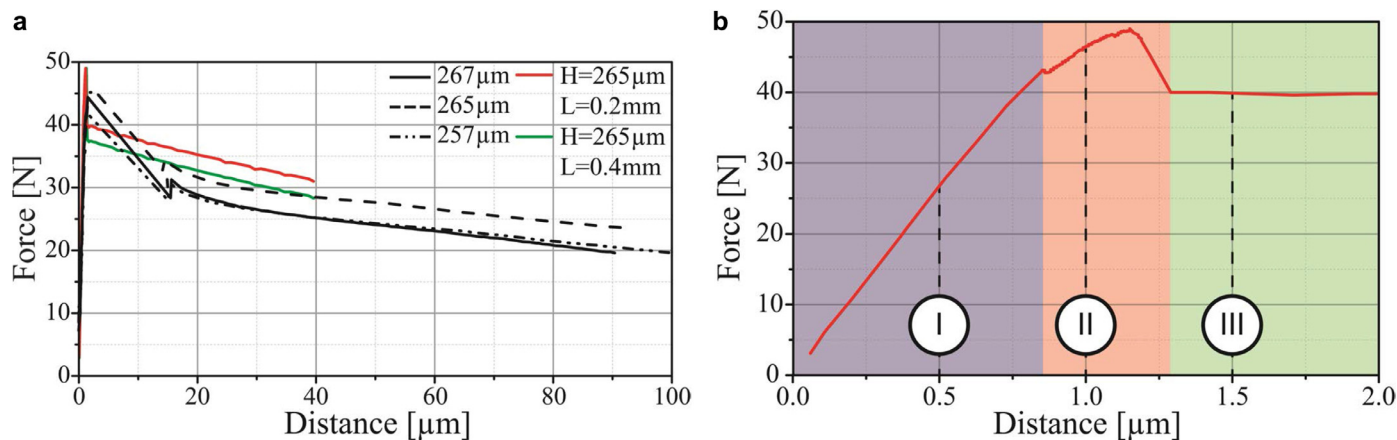


Fig. 12. (a) Force-displacement curves of push-out tests showing experimental curves of CVD W_f/W for similar thicknesses and simulated curves for different support diameters. (b) Inset of the simulated curve for $H=265 \mu\text{m}$ and $L=0.2 \text{mm}$. The color corresponds to the three stages of a push out test. The dotted lines refer to curves in Fig. 11.

Therefore, samples fabricated via powder metallurgical methods (e.g. HIP) differ significantly in their push-out behavior when compared to samples produced via CVD (Figs. 12 and 4), where presumably the assembly process allows for a stress-free growth of the matrix leading to a low initial pressure. This means that the frictional properties of the interface will severely influence the performance of W_f/W composites. Future iterations of the simulation model will also take those considerations into account and include the more complex interface properties of HIP W_f/W .

If the general shape of the force-displacement curves of HIP and CVD single-fiber W_f/W holds true one can see a distinct difference in the behavior after complete debonding. In the case of CVD a sudden drop in the load can be observed after debonding. Whereas for W_f/W produced via HIP a steady transition between the debonding and frictional phase can be seen.

With the fact that every sample is unique, it is rather difficult to draw final conclusions from push-out tests of HIP W_f/W , in terms of mechanical properties like τ_d . This is mainly due to the uncertainty and local variation of the interface properties. However, it is obvious that the deformation caused by HIP leads to a strong interface when compared to CVI W_f/W also utilizing Er_2O_3 as the interface material.

In order to finally bring the model and the experimental results together synchrotron tomography and diffraction studies of W_f/W are in preparation, also to clarify the possible influence of residual stresses. More detailed material parameter studies and micro structural analysis of both CVD W_f/W and PM W_f/W are required to adapt the model to the actually obtained results.

When moving to the powder metallurgical route extra energy dissipation might be expected. As one of the main mechanisms of W_f/W is fiber pull-out after matrix cracking, PM W_f/W might actually perform better with relation to energy dissipation as CVD W_f/W . As a next step the production of multi-fiber PM W_f/W is ongoing.

Acknowledgment

This work has been carried out within the framework of the EUROfusion Consortium and has received funding from the Euratom research and training programme 2014–2018 under grant agreement No 633053. The views and opinions expressed herein do not necessarily reflect those of the European Commission. We are very thankful for the intensive collaboration within the W_f/W team and thank the team at the IEK-1 for providing the HIP.

References

- [1] R. Pitts, et al., *J. Nucl. Mater.* (438) (2013) S48.
- [2] J.W. Coenen, et al., in: *Proceedings of the 15th International Conference on Plasma-Facing Materials and Components for Fusion Applications (PFMC-15)*, 2015.
- [3] R. Lässer, et al., *Fusion Eng. Des.* 82 (5) (2007) 511–520.
- [4] H. Bolt, et al., *J. Nucl. Mater.* 307–311 (1) (2002) 43–52.
- [5] J. Du, J.-H. You, T. Höschen, *J. Mater. Sci.* 47 (11) (2012) 4706–4715.
- [6] J. Riesch, et al., *Phys. Scr.* 2014 (T159) (2014) 014031.
- [7] M. Launey, R. Ritchie, *Adv. Mater.* 21 (20) (2009) 2103–2110.
- [8] G. Czel, M. Wisnom, *Compos. Part A: Appl. Sci. Manuf.* 52 (0) (2013) 23–30.
- [9] J. Reiser, et al., *Adv. Eng. Mater.* 17 (4) (2014) 491–501.
- [10] J. Reiser, M. Rieth, *Fusion Eng. Des.* 87 (5–6) (2012) 718–721.
- [11] A.A. Németh, et al., *Int. J. Refract. Met. Hard Mater.* 50 (0) (2015) 9–15.
- [12] A. Hohenwarter, R. Pippin, *Philos. Trans. R. Soc. Lond. A: Math., Phys. Eng. Sci.* 373 (2038) (2015).
- [13] P. Zhao, et al., *Int. J. Refract. Met. Hard Mater.* (2016). Submitted for publication.
- [14] J. Riesch, et al., *Acta Mater.* 61 (19) (2013) 7060–7071.
- [15] R. Neu, et al., *J. Fusion Eng. Des.* (2016). In Press.
- [16] J. Riesch, et al., *Phys. Scr.* 2016 (T167) (2016) 014006.
- [17] B. Jasper, et al., *Mater. Sci. Forum* 825–826 (2015) 125–133.
- [18] K. Shimoda, et al., *Compos. Sci. Technol.* 68 (1) (2008) 98–105.
- [19] J. Du, et al., *Compos. Sci. Technol.* 70 (10) (2010) 1482–1489.
- [20] C.R. Ananth, N. Chandra, *J. Compos. Mater.* 29 (11) (1995) 1488–1514.
- [21] M. Kallas, et al., *J. Mater. Sci.* 27 (14) (1992) 3821–3826.
- [22] D.K. Shetty, *J. Am. Ceram. Soc.* 71 (2) (1988) C–107–C–109.
- [23] C. Liang, J. Hutchinson, *Mech. Mater.* 14 (3) (1993) 207–221.
- [24] J.-H. You, et al., *Int. J. Solids Struct.* 46 (25–26) (2009) 4277–4286.